CrossMark

# A high-force and high isolation metal-contact RF MEMS switch

Peigang Deng[1] · Ning Wang[1] · Feng Cai[1] · Longquan Chen[2]

**Abstract** A simple structure, high-force and high isolation metal contact RF MEMS switch was fabricated based on micro electroplating technology, and the mechanical and RF performance of the switch were measured. After release and annealing, the switch's cantilever beam showed a tip-up of less than 1 μm over the beam length of 485 μm, indicating a good stress control and thermal stability of the electroplated gold. The pull-in voltage and the switching characteristics at different temperatures, ranging from 25 to 90 °C, were investigated. A fast, stable and temperature independent switching process was observed as the actuation voltage was 10% larger than the pull-in voltage. Based on the classical cantilever beam model, both the electrostatic actuation force and the return force of the switch were larger than 1000 μN, and the extracted effective spring constant of the free-standing beam was 718 N/m. Cold RF tests were carried out at various temperatures by a network analyzer, and we found that temperature showed very less influence on the insertion and isolation of the switch in the present case. At 25 °C, the insertion loss was −0.13 dB at 10 GHz, and was lower than −0.3 dB over the 0.05−20 GHz frequency range. The isolation was −36 dB at 10 GHz, and was higher than −27 dB over the entire scanning frequency range. The high isolation performance is consistent with a lumped-element equivalent circuit analysis of the switch.

✉ Longquan Chen
  lqchen@swjtu.edu.cn

1  School of Science, Wuhan Institute of Technology, Wuhan 430205, People's Republic of China

2  School of Mechanics and Engineering, Southwest Jiaotong University, Chengdu 610031, People's Republic of China

## 1 Introduction

Currently, most of the commercial radio frequency (RF) switches rely on either traditional semiconductor technology or micro-electro-mechanical-system (MEMS) technology. As compared with the semiconductor solid switches (for example pin diodes or FETs), RF MEMS switches offer many key advantages, such as wideband, ultralow insertion loss, high linearity, negligible power consumption, and high power handling capability (Rebeiz 2003). RF MEMS switch has been investigated for many years, and as a widely-used device, it can be applied in a RF circuits independently or combined with other electric devices. The potential application of the MEMS switch includes switchable routing networks in RF system front-ends, connection to capacitor banks, phase shifters, and space-based applications, etc. (Jaafar et al. 2014; Chiou et al. 2012; Muniraj and Sathesh 2011; Pirmoradi et al. 2015; Yuan et al. 2008).

Since the MEMS switch usually has free-standing cantilever beam and moving part, its micro fabrication process is very complicated. Among which, the thickness control, uniformity and residual stress control of the free-standing beam, the flatness of the sacrificial layer, the release process, and the mechanical and electric properties of the contacts are all the key processes affecting the performance of the switch. Therefore, despite the advantages, the reliability of MEMS switches is of major concern for long-term and broad applicability (Shankar et al. 2011; Jan et al. 2014). Compared with capacitive MEMS switch, metal-contact resistive MEMS switch actuated by electrostatic force offers extremely low power consumption and bias networking simplicity (Pisheh et al. 2009). Although metal-contact switches have demonstrated excellent RF performance, they are very sensitive to the internal residual stress of the metal during its micro-fabrication process. The residual

stress could induce the buckling of the free-standing metal beam either after release or back-end process, which in turn could result in such malfunction of the switch as gate short, high pull-in voltage etc. In particular, high temperature or significant temperature variations in some applications, for example aircraft and satellites communication in space, can lead to serious issues of the MEMS switch. Under these situations the effect of working temperature on the switch performance is of a major concern. Preliminary results have been reported on the temperature effects on MEMS switch's beam deformation, pull-in voltage variation and adhesion of the contacts (Mulloni et al. 2016; Alcheikh et al. 2014). Therefore, a thermally-stable free-standing beam with low residual stress would be of great importance in terms of a reliable MEMS switch.

The adhesion of the contacts and the contact resistance increase over cycles are also main concerns for metal contact switch, which can directly lead to the failure of the switch. As the switch works, the metal contacts close and open frequently. Especially, under high RF power situation, the joule heating can lead to the temperature increase of the contacts, which facilitates the adhesion of the contacts. Contaminants or moistures introduced during an undesirable switch packaging process can make this issue even more serious. The switch must overcome this adhesion force with its own return force during a proper opening action. The return force of the switch is determined by the strain energy restored in the deformed free-standing beam as the actuation voltage is removed. If the switch beam is very "soft" (with a small stiffness or spring constant), the return force may be lower than the adhesion force. Thus the switch fails with stiction. Previous research has shown that the return forces required to separate switch contacts are 100–2700 μN for gold, 300 μN for a gold-nickel alloy, and 100 μN for rhodium (Schimkat 1999; Mercado et al. 2003; Oberhammer and Stemme 2006). Typically, the downward displacement or deformation of an electrostatically driven switch beam is about 1 μm, and accordingly the required spring constant of the beam can be 100–2700 N/m for commonly used gold. Apparently, a "hard" switch beam with large spring constant can provide a large return force and thus lower the susceptibility for permanent contact stiction. In addition, this kind of "high-force" switch design may also decrease the contact resistance and therefore improve the RF performance of the switch, because the large contact force increases the size of the contact spot. Of course, a high-force switch needs a large actuation voltage and thus increases the burden of the charge pump. However, as the power consumption for driving the switch is ultra low, commercial RF MEMS switches usually choose high force operation to ensure their reliability. For example, the recommended actuation voltage is 90 V for the metal contact switch provided by Radant MEMS, which is one of the very few successful RF MEMS switch commercial companies (Newman et al. 2008).

In some applications, such as mobile communication systems and automatic test equipments, high isolation of the RF switch is demanded, otherwise the leakage of the RF signals will considerably decreases the RF system performance. In recent years, efforts have been devoted in developing novel design of the RF switch with high isolation (Jang et al. 2011; Sim et al. 2016). However, this kind of switches usually have complicated structures and thus the micro fabrication process control, manufacture cost and yield will be affected. An alternative way is to generate a combined series/shunt switch configuration, as have been commonly used in wideband PIN diodes and FETs (Mafinejad et al. 2013). However, the weight, size and bias circuit of this kind of switch matrix might also be complicated and not applicable in some situations.

In this study, we will report our recent research on developing a simple structure, high isolation, high-force and thermally-stable metal contact RF MEMS switch. The RF in and out signal lines are designed as the two separate contact pads of the switch. A lumped-element equivalent circuit analysis indicates that this design can reduce the RF coupling and thus increase the isolation at the switch-off state. As the moving part of the switch, a 8.8 μm thick free-standing gold beam is electroplated, which makes the switch mechanically robust. The micro electroplating process is optimized (bath temperature, pH of the base solution and current density), and especially, trivalent arsenic additives are used to make a fine-grain gold deposition. With the optimized micro fabrication process, the switch is insensitive to stress and temperature. After release, the buckling of the free-standing beam is examined by a surface profiler, and the results show a tip-up of less than 0.2% along the switch length of around 485 μm. The pull-in voltage and the switching time are measured under different temperature, ranging from 20 to 90 °C. We find that if the actuation voltage is large enough, the temperature shows less influence on the on/off switching time. Due to the high force design, the actuation force and the return force of the switch are 1277 and 1149 μN, respectively, and the effective spring constant of the free-standing beam is 718 N/m. Finally, cold RF tests of the switch are conducted by a network analyzer, and both the insertion loss and isolation within the range of 0.05–20 GHz are measured. The MEMS switch shows a low insertion loss of −0.13 dB and a high isolation of −36 dB at 10 GHz, respectively. The defects of the switch contacts after the RF tests are examined by taking scanning electron microscopy. A preliminary analysis shows that the Au contacts are easy to be damaged due to mechanical impact, scratch and friction.

**Fig. 1** Images of the metal contact RF MEMS switch. **a** Overview of the MEMS switch. **b** Venting hole in the cantilever beam of the switch. **c** Metal contact of the switch
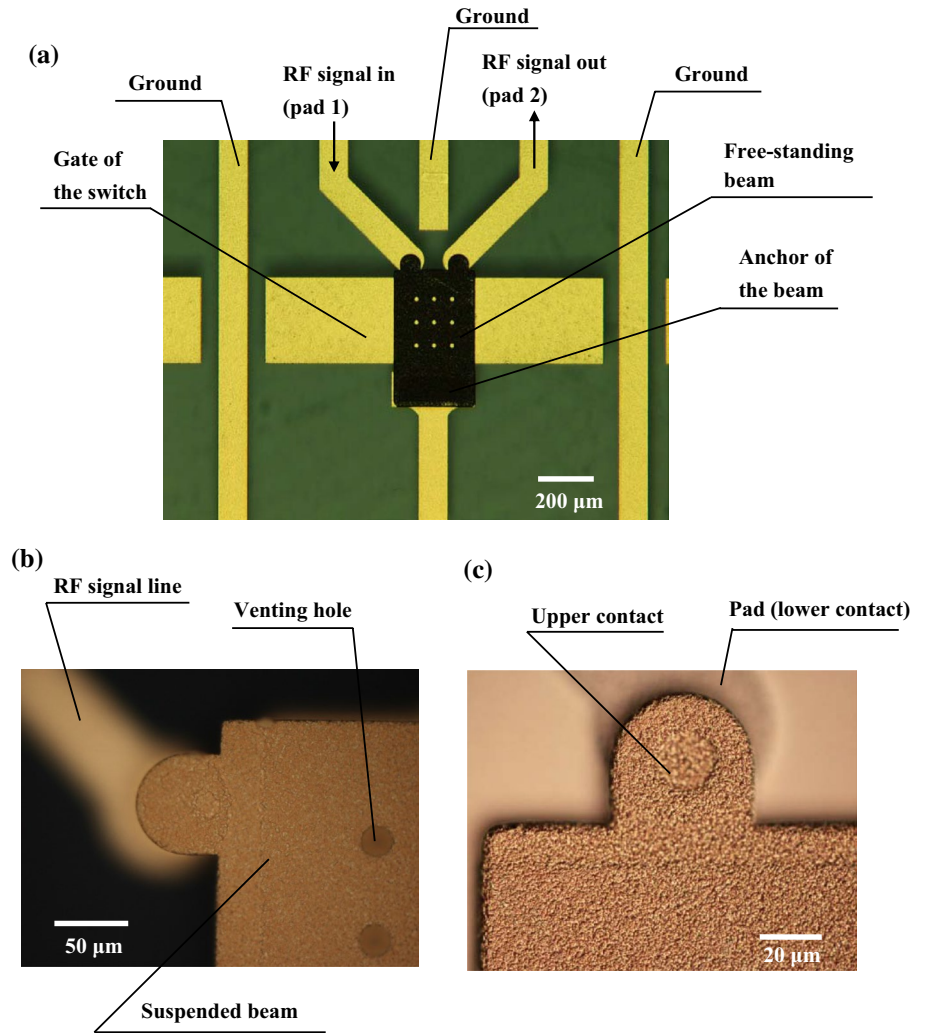


## 2 Manufacturing procedure

### 2.1 Design

The present paper focuses on improving the RF performance (high isolation and low insertion loss) of a MEMS switch with high-force design (high actuation force and return force). Figure 1 shows the images of our MEMS switch, and Fig. 2a shows the schematic diagram of it. A coplanar waveguide was designed for the transmission of the RF signal, and the RF input port (pad 1) and RF output port (pad 2) were designed as the two pads of the two lower contacts the switch, respectively. As the switch worked, a electrostatic potential was exerted in between the gate and beam of the switch, and as a result the free-standing beam moved downwards due to electrostatic force until the two upper contacts reached the metal pads of the RF signal lines (refer to Fig. 2a). Thus, the switch was at the "on" state, and the RF signals could pass through pad 1 and pad 2. When the electrostatic potential was removed,

the free-standing beam moved upwards due to the return force. The pad 1 and pad 2 were electrically disconnected, and the switch was at the "off" state. As shown in Fig. 1b, some venting holes were uniformly distributed in the beam to provide a proper damping as the beam moved. Figure 1c illustrates the details of the metal contact at the end of the switch beam, and the metal pad at the end of the RF signal line.

The switch isolation is defined by the coupling capacitance between electrodes when the switch is at the "off" state. To illustrate the high isolation design of the present switch, a lumped-element equivalent circuit analysis was performed. As shown in Fig. 2a, the RF input line and the RF output line were designed as the two separate metal pads on the substrate, respectively. While in a conventional switch, the RF input line is usually connected to the free-standing beam, and the output line is connected to the pads, or vise verse (Rebeiz 2003). Figure 2b, c are the lumped element equivalent circuits of the present switch and a conventional switch, respectively. $C_g$ is the capacitance between the beam

**Fig. 2** **a** Schematic diagram of the present MEMS switch. **b** The equivalent circuit of the present switch at off-state. **c** The equivalent circuit of a conventional switch at off-state
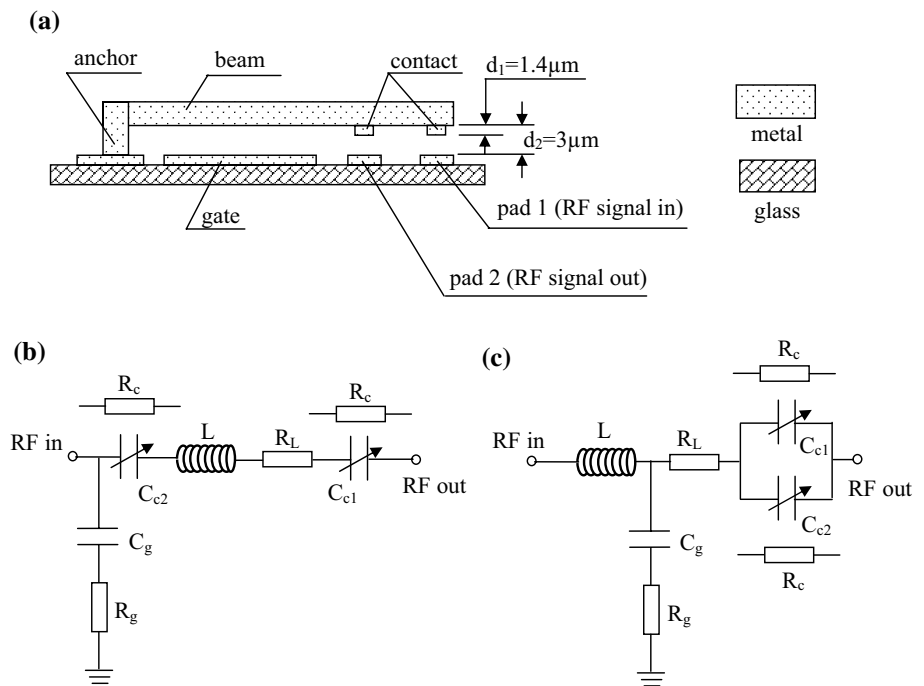


and gate, and $R_g$ is the resistance between the gate and the ground. Note that $R_g$ is usually a high resistance resistor (~100 kΩ) of the driving circuit to prevent the direct short of the RF signal to the ground (Newman et al. 2008). L and $R_L$ are the inductance and resistance of the RF transmission line, which is usually made of gold (refer to Fig. 1). $C_c$ is the capacitance between the pad and the contact at switch off-state, and it converts to a very small resistance (contact resistance, $R_c$) at the switch on-state. Therefore, the equivalent circuit can be further simplified as just a capacitance ($C_c$) at switch off-state, and a inductance (L) in series with resistance ($R_L + R_c$) at switch on-state. The former affects the isolation and the latter affects the insertion loss of the switch. Apparently, in the present design, there are two capacitance in series ($C_{c1}$ and $C_{c2}$ in Fig. 2b) at the off-state, which decreases the equivalent capacitance as compared with that in a conventional design ($C_{c1}$ and $C_{c2}$ in Fig. 2c). Furthermore, for the present high-force switch design, the gap between the pad and the contact is 1.6 μm ($d_2 - d_1 = 1.6$ μm, Fig. 2a), while in a conventional design it is typically less than 1 μm. Such a design also decreases the capacitance of $C_{c1}$ and $C_{c2}$. Therefore, by increasing the impedance of the switch at off-state, the present switch design can reduce the coupling of the RF signal from the input to output end, and thus show a better isolation performance.

## 2.2 Micro fabrication

Figure 1 shows the images of the metal contact RF MEMS switch. Pyrex 7740 glass (Corning Inc., NY, USA) was

utilized as the substrate for the MEMS switch, which could provide substantially lower high-frequency losses than the silicon substrates used in other MEMS switches. The micro fabrication started with a TiW/Au (100 nm/150 nm) sputtering on the glass wafer, which acted as the seed layer for the electroplating process. Photoresist AZ4903 (Clariant, USA) was then spin coated, exposed, developed and baked to form the electroplating mold.

Figure 3 shows the experimental set-up of the gold micro electroplating system. In our previous study, three-dimensional gold micro electrode pairs have been electro-plated in microfluidic chips, in which the bio-compatible surface treatment are of major concern (Deng et al. 2012, 2014). In the present study, however, emphasis will be put on the uniform grain size and low stress control. As an alkaline and non-cyanide plating solution, NEUTRONEX 309 (Cookson Electronics, USA) was used as the plating solution. During the electroplating process, a beaker containing the plating solution was placed on a hot plate with a magnetic stirrer. The stirring during the plating process could enhance the mass transport in the bath. A multi-meter was serially connected with a Keithley 224 programmable current source (Keithley, USA) to monitor the plating current. A silicon wafer deposited with sputtered platinum acted as the anode. The wafer to be electroplated acted as the cathode, and with its backside covered with photoresists. To deposit low stress gold layer, we optimized the electroplating process and maintained the plating solution at a pH of 9.5, a bath temperature of 50 °C, and a DC electroplating mode with a current density of 1.1 mA/cm². In addition, to
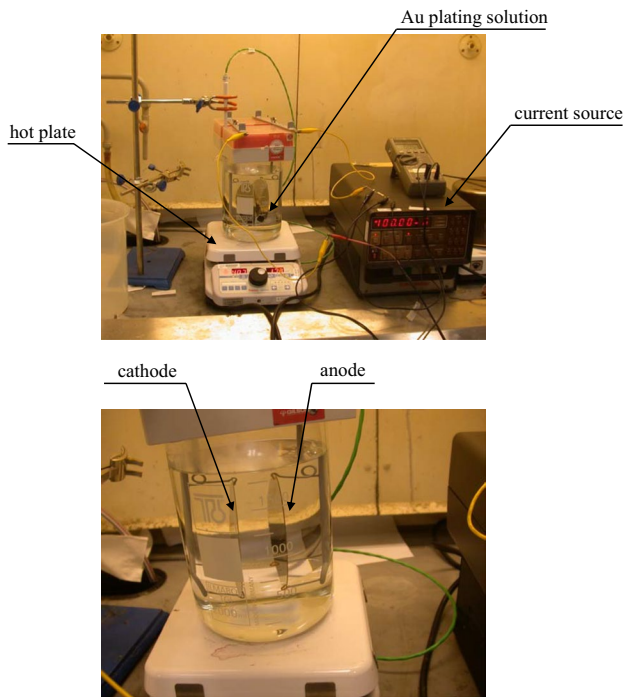
**Fig. 3** Experimental set-up of the Au micro electroplating system

generate fine-grain gold, trivalent arsenic was added in the plating bath with an optimized concentration of 10 ppm, which can facilitate a uniform gold nucleation during the electroplating process. With the optimized process, a 1.5-μm thick Au was electroplated on the seed layer to form the RF signal transmission line, the ground, the gate of the switch and the anchor of the free-standing beam, as shown in Fig. 1a. Note that a thick signal transmission line generates less loss as the RF signal passes, especially at the contacts of the switch under high RF power.

After the first layer gold electroplating, the Au and TiW seed layer outside the switch area was wet etched by potassium iodide at room temperature and hydrogen peroxide at 60 °C, respectively. After that, a TiW/Al (100 nm/3 μm) sacrificial layer was deposited. Both photoresist and some metals, for example aluminum, copper, nickel and zinc, can be used as the sacrificial material. In the present study, aluminum was chosen as the sacrificial layer for its low temperature sputtering process, good thickness control capability, high electric conductivity and good etch selectivity to other materials we used. The 3 μm-thick Al was sputtered by two steps: firstly, a 1.4 μm-thick Al was sputtered and then the Al at the contact area was wet etched by phosphoric acid at 50 °C to realize a dimple at the tip of the contact (refer to Figs. 1c, 2a). Secondly, another 1.6 μm-thick Al was sputtered on top of the first Al layer. After the deposition of the sacrificial layer, another TiW/Au (100 nm/150 nm) was sputtered as another seed layer.

Then, the Au/TiW/Al/TiW metal layers at the anchor of the free-standing beam was wet etched sequentially to expose the 1.5 μm-thick Au, on which the beam stood (Figs. 1a, 2a). Thereafter, a 8.8 μm-thick Au was electroplated as the cantilever beam of the switch with a dimension of $266 \times 485$ μm$^2$. A relatively thick beam was utilized to make the switch mechanically robust. Although a thick cantilever beam may increase the pull-in voltage of the switch, it can generate a large return force as the switch opens and thus reduce the stiction of the switch contacts. As shown in Fig. 1c the grain size of the electroplated Au is very small and uniform with the optimized micro electroplating process. The last step of micro fabrication was the release process. It began with the wet etch of the sputtered TiW/Au seed layer, and followed with the wet etch of the sputtered Al sacrificial layer, and finally the wet etch of the sputtered TiW layer. Since the switch was mechanically robust, there was no stiction of the free-standing beam after release. After the micro fabrication, the glass wafer was diced, and the MEMS switch was attached to a PCB board and wire bonded.

## 3 Results and discussions

### 3.1 Thermal stability of the free-standing beam

To test the thermal stability of the free-standing Au beam, the switch was annealed 1 h in the oven at 300 °C after release. Recrystallization of the electroplated Au was anticipated during the annealing process for stress release. A surface profiler (Dektak 150, Veeco Instruments Inc, USA) was employed to scan the Au beam to examine its flatness before and after annealing. There is no measurable deformation of the beam before annealing. After annealing, as illustrated in Fig. 4, the suspended beam showed a tip-up of less than 1 μm over the beam length of 485 μm, indicating the good stress control and thermal stability of the electroplated gold beam.

### 3.2 Testing electrical circuit and the pull-in voltage at various temperatures

A testing electrical circuit for the MEMS switch was designed as shown in Fig. 5. As an electrostatic potential was imposed in between the "gate" and "beam" of the switch, the pad 1 and pad 2 were electrically connected and the switch was at the on-state. After the removal of the electrostatic potential, the pad 1 and pad 2 were electrically disconnected and the switch was at the off-state. To study the pull-in voltage and the switching time of the switch, a DC test was carried out. A high voltage supply unit (PS310, Stanford Research Systems, USA) was connected to $V_{act}$
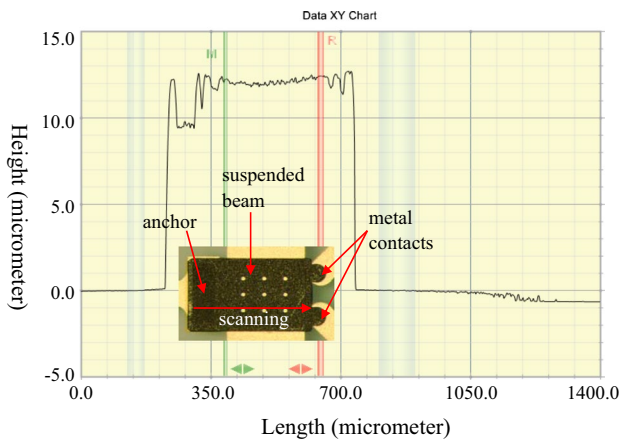
**Fig. 4** Thermal stability test of the free-standing beam of the MEMS switch after annealing in oven for 1 h at 300 °C

end for electrostatic actuation of the switch. A DC voltage supplier (V = 3 V) was connected to pad 1 of the switch, and pad 2 was grounded. The voltage at R2 was measured by a data acquisition card (PCI 6110, National Instrument, TX, USA). In addition, to investigate the temperature effects on the switching behavior, the MEMS switch was put on a hot plate with a thermocouple attached to the glass substrate of the switch. The temperature of the switch was maintained by adjusting the power of the hot plate until it reached the desired value.

Figure 6 shows the measured pull-in voltage of the switch as a function of temperature, ranging from 25 to 90 °C. Note that the measurements were performed before and after annealing, in which the switch was baked in oven for 1 h at 300 °C after release. The pull-in voltage at room

temperature (25 °C) was about 88 V before annealing and 83 V after annealing. Since the present switch is of a high-force design, it is not surprise that a large necessary pull-in voltage is required. The electrostatic actuation force based on a simplified cantilever beam model can be calculated as:

$$F_a = 2\frac{\varepsilon_0 V_p^2 A}{g_0^2},\tag{1}$$

where $V_p$ is the actuation voltage, $g_0$ and $A$ are the gap and the overlapping area between the beam and the gate, $\varepsilon_0$ (= $8.85 \times 10^{-12}$ F/m) is the dielectric constant of air. Taking $V_p = 83$ V, $g_0 = 3$ μm and $A = 9.43 \times 10^{-8}$ m$^2$ into Eq. (1), we can get $F_a = 1277$ μN.

Besides a large actuation force, the present switch should also have a large return force as the switch opens, so as to reduce the possibility of the stiction of the switch contacts. The closed-form analytical expression for the pull-in voltage $V_p$ can be expressed as (Pamidighantam et al. 2002):

$$V_p = \sqrt{\frac{8K_s g_0^3}{27\varepsilon_0 A}},\tag{2}$$

where, $K_s$ is the effective spring constant of the free-standing beam. Taking the above mentioned values of $V_p$, $g_0$ and $A$ into Eq. (2), we can get $K_s = 718$ N/m. At the switch on-state, the downwards displacement of the beam under the electrostatic force could be estimated as $\Delta g = d_2 - d_1 = 1.6$ μm (refer to Fig. 2a), and the resultant return force, $F_r$, can be calculated as: $F_r = K_s \Delta g = 1149$ μN. Note that the return force of the present switch is very large as compared with many other
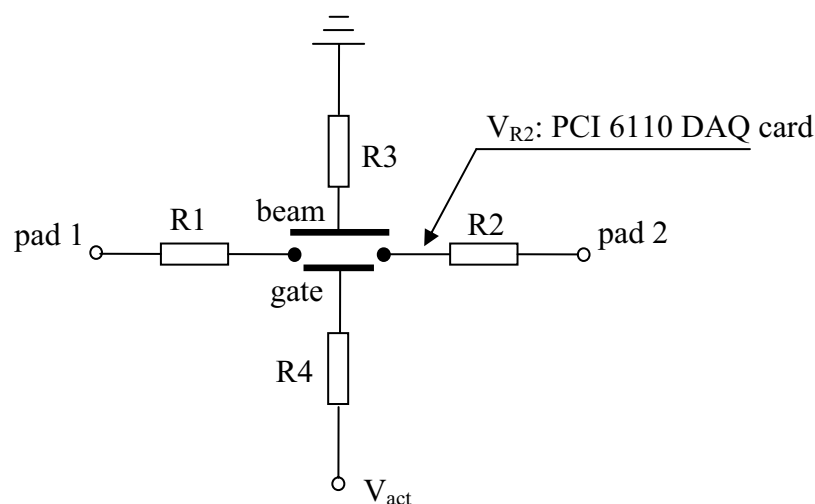


**Fig. 5** Schematic diagram of the testing electrical circuit of the MEMS, switch. For DC test: V = 3 V at pad 1, R1 = R2 = R3 = R4 = 100 kΩ. For RF performance test, R1 = R2 = 0, R3 = R4 = 100 kΩ
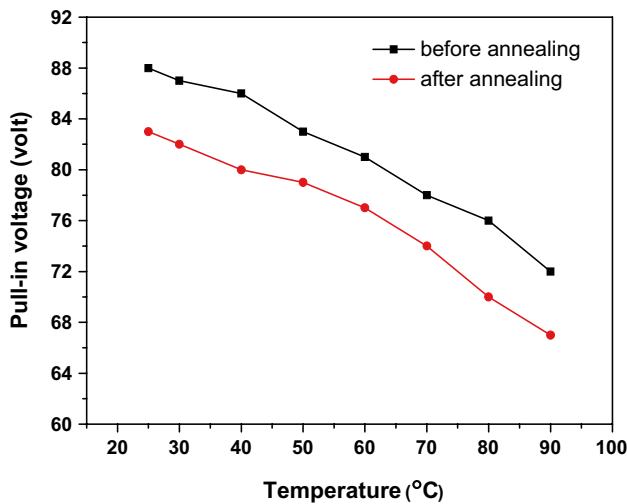
**Fig. 6** Measured pull-in voltage as a function of temperature for the switches before and after annealing

cantilever switches, in which it is in the range of 100–1000 µN (Oberhammer and Stemme 2006).

Figure 6 also shows that the pull-in voltage decreased dramatically with the increase of the temperature for both switches with and without annealing. At the same operation temperature, the pull-in voltage decreased by ~5% for switches underwent annealing process, attributed mainly to the change of the mechanical properties of the gold because the beam deformation after annealing was neglectable for the present case.

### 3.3 Switching characteristics of the switch

Switching time is another important parameter of a MEMS switch. To measure the switch-on time, the actuation voltage $V_{act}$ was simultaneously input to the gate of the switch and the PCI 6110 data acquisition card to trigger the voltage recording at R2, referred as $V_{R2}$ in Fig. 5. The time duration of $V_{R2}$ increased from 0 to 1 V was regarded as the switching-on time. Similarly, as $V_{act}$ was removed, the time duration of $V_{R2}$ decreased from 1 to 0 V was regarded as the switching-off time. Figure 7 shows the switching-on time and switching-off time of the switch under different actuation voltage and working temperatures. We imposed different actuation voltages on the switch, equal to and larger than the pull-in voltage (up to 20% larger than the pull-in voltage), and the actuation voltage is normalized by the corresponding pull-in voltage at each temperature.

As shown in Fig. 7a, when the actuation voltage was set to be the pull-in voltage at each temperature, the switching-on time was very long (23–98 ms) at all temperatures, and it increased with the temperature. The longest switching-on time (98 ms) was observed at the highest temperature,
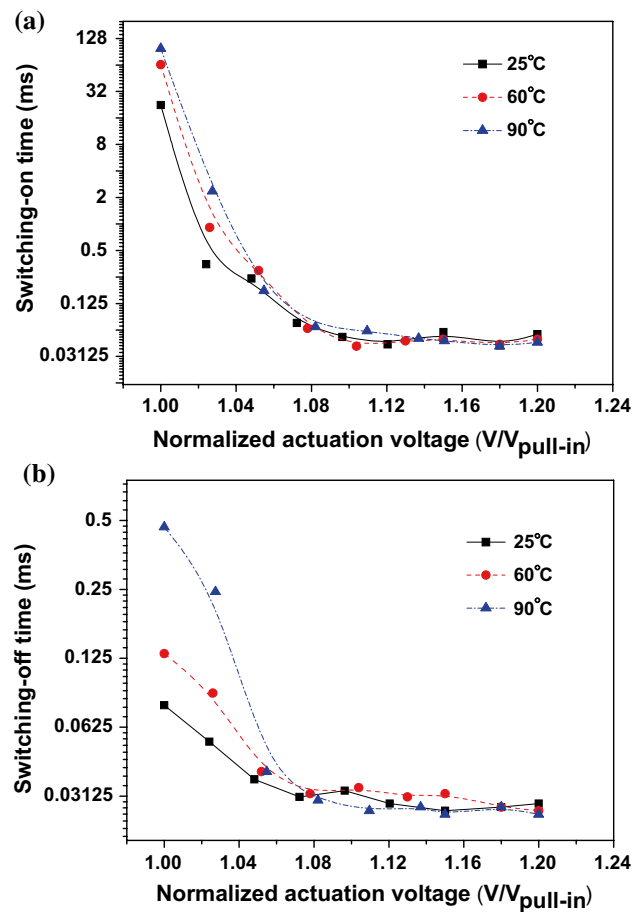


**Fig. 7** Measured switching time as a function of the normalized actuation voltage at different temperatures ($V_{pull-in}$ is the pull-in voltage at each corresponding temperature). **a** Switching-on process. **b** Switching-off process

90 °C. However, when the actuation voltage was raised to be 10% larger than the pull-in voltage for each temperature, the switching-on time decreased dramatically and shortened to be ~50 µs for all temperatures. These findings imply that as compared to the temperature effects, the actuation voltage will be the dominate factor if it is high enough (about 10% larger than the pull-in voltage in the present case). On the other hand, the temperature can effectively affect the switching-on process only when the actuation voltage is just around the pull-in voltage.

In general, the switch closing process depends on the electrostatic actuation force, return force due to the stain energy of the beam, air damping underneath the beam, bounce due to the mechanical impact of the contacts, contact force and the adhesion force of the contacts. When the actuation voltage was set to be the pull-in voltage, the switch closed but the closing event lasted for a relatively long time. This is because the electrostatic actuation force, which needs to overcome the resistance from the return

force, air damping, impact bounce force and the contact force, was not large enough for a fast and stable switch closing in this case. It is worth to note that non-linear impact dynamics of the MEMS switch has been theoretically studied for better understanding this phenomenon (Lii and Murphy 2010).

The switching-off process, as illustrated in Fig. 7b, shows the similar temperature influence as the switching-on process. Under low actuation voltage, the switching-off time was large, and it increased with temperature. The longest switching-off time (0.47 ms) was observed at the highest temperature, 90 °C. Besides the return force, the adhesion force of the contacts is also an important factor affecting the switching-off time, which depends on the area of the contact dimple and the temperature as well. At high temperature, the gold became softer and the contact area became larger. Thus, a large adhesion force and hence a relatively long switching-off time could be expected, which is consistent with the experimental results as shown in Fig. 7b. However, the switching-off time was all around 30 μs under high actuation voltage (about 10% larger than the pull-in voltage in the present case), independent of the temperature. Apparently, under large actuation voltage, the cantilever beam deformed larger and more strain energy was accumulated. Thus, as the actuation voltage was removed, the return force was large and the beam quickly left the contact surface leading to a short switching-off time.

From Fig. 7a, b, it is very clear that slow switching process, both on and off, occurred when the actuation voltage was set to be the pull-in voltage. And both the on/off time increased dramatically with the working temperature. However, a fast and temperature-independent switching process could be realized when the actuation voltage was set to be at least 10% larger than the pull-in voltage. Further increase of the actuation voltage, up to 20% larger than the pull-in voltage, showed less influence on the switching process. These findings ca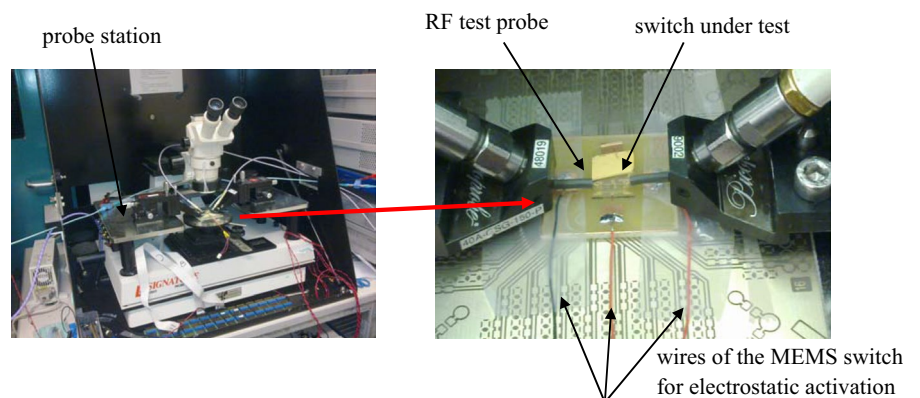n provide guidance to properly choose the actuation voltage of the electrostatic driven RF MEMS switch for a fast and reliable switching process.

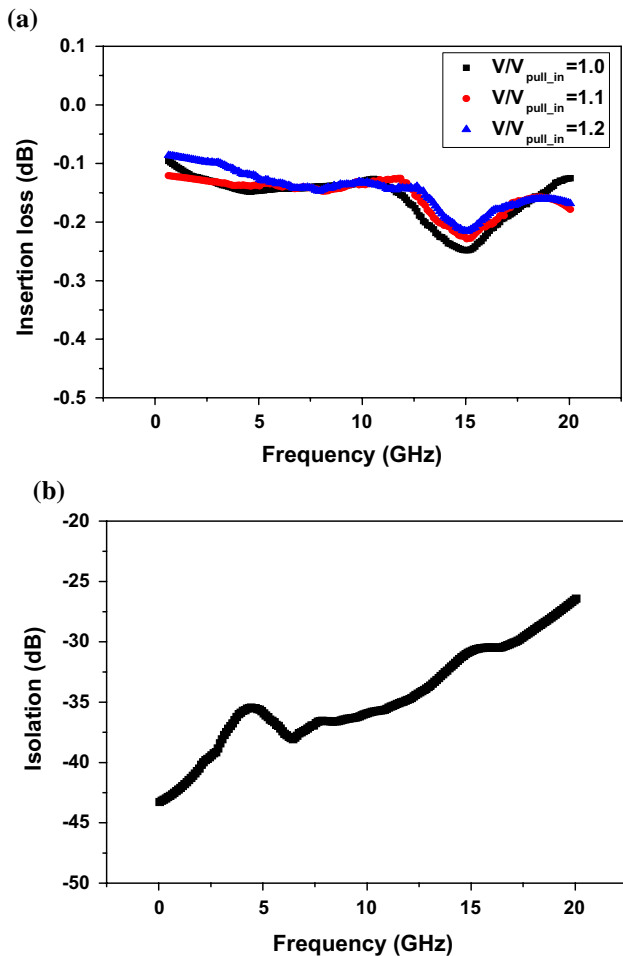### 3.4 RF performance of the switch

To test the RF performance of the switch, an experimental set-up was established as shown in Fig. 8. The packaged switch was mounted on a probe station (SignaTone S1160, Signatone, USA). A pair of high performance microwave RF probes (Picoprobe 40A, GGB Industries, USA) were put on the input port (pad 1) and output port (pad 2) of the switch, respectively. S-parameter measurements were performed over the 0.05–20 GHz frequency range using a network analyzer (Agilent 8720ES, Agilent Technologies, USA). During the test, the pad 1 and pad 2 of the switch were connected to the network analyzer, R1 and R2 were zero, and a high voltage potential was imposed on the $V_{act}$ end for switch actuation (refer to Fig. 5).

Cold RF test was carried out at 25 °C in air, in which the RF signal was applied to the switch after it was at the on-state, and removed before it was at the off-state. Figure 9a shows the measured insertion loss as a function of frequency, in which the actuation voltage was set as the pull-in voltage, 10 and 20% larger than the pull-in voltage, respectively. The measurement shows that the actuation voltage has little influence on the insertion loss, although it can affect the mechanical performance of the switch very much. This implies that the contact resistance of the switch under different actuation voltage was very similar. The insertion loss is −0.13 dB at 10 GHz, and is lower than −0.3 dB over the entire scanning frequency range. Figure 9b shows that the measured isolation is −36 dB at 10 GHz, and is higher than −27 dB over the entire scanning frequency range. Note that RF tests under various temperatures, ranging from 25 to 85 °C, and with the corresponding actuation voltage chosen from Fig. 6 were also performed in the present study. We found that temperature showed very less influence on the insertion and isolation

**Fig. 8** Experimental set-up of the RF test system of the RF MEMS switch

**(a)**



**(b)**



**Fig. 9** S-parameter measurement of the switch. **a** Insertion loss of the switch under different actuation voltage. **b** Isolation of the switch

capacitance of the switch because the beam is thermally stable. As to the on-state contact resistance, theoretically the temperature could affect it because of the change of the contact force and contact area. However, since gold is a very good conductive material, and the imposed actuation voltage was just the pull-in voltage at each temperature, the contact resistance change due to temperature was very small in the present case. Researchers have found that high temperature can facilitate the buildup of contamination on the contact surface gradually in an undesired hermetic package (Toler et al. 2013). Under this situation, the RF performance can be affected by temperature in terms of the long-time running of the switch. After the tests, the cantilever beam of the switch was carefully flipped over, and Fig. 10 are the SEM photographs of the switch contacts. Apparently, mechanical impact, scratch and friction during each contact led to obvious dents on both the upper and lower contact surfaces, and some small gold pieces detached from the contact surface. Those dents and small gold pieces might cause stiction or contamination on the contacts of the switch. Many investigations have been taken to study the contact physics in detail, and the readers are referred to those papers on this special issue of MEMS switch (Toler et al. 2013; Gilbert et al. 2008).

## 4 Conclusions

A high force, high isolation metal contact RF MEMS switch was designed, fabricated and tested. Gold micro electroplating process was developed and optimized for low stress and thermally stable free-standing beam. The pull-in voltage and the switching characteristics at different temperatures were investigated. A fast, stable and temperature independent switching process was observed at high actuation voltages. In addition, the present switch showed a mechanically hard free-standing beam with an effective spring constant of 718 N/m, and both the actuation force and the return force of the switch were larger

of the switch. As discussed in Sect. 2.1, the equivalent circuit of a switch can be simplified as a off-state capacitance between the pad and the contact, and a inductance of the transmission line in series with resistance of the transmission line and the contact resistance at the switch on-state. The temperature can hardly affect the off-state equivalent

**Fig. 10** Typical SEM photographs of the switch contacts. **a** Upper contact. **b** Lower contact

**(a)**                                                                              **(b)**
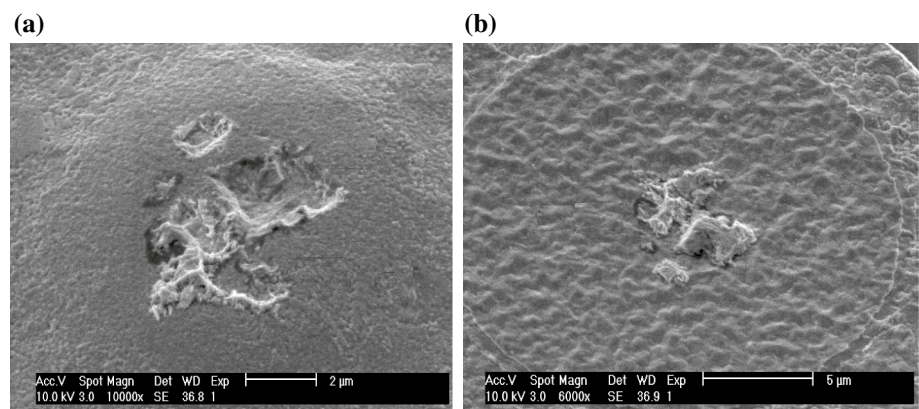
than 1000 μN. Cold RF tests were conducted by a network analyzer and the working temperature showed very less influence on the insertion and isolation of the switch in the present case. At 25 °C, the insertion loss was −0.13 dB at 10 GHz, and was lower than −0.3 dB over the 0.05–20 GHz frequency range. The isolation was −36 dB at 10 GHz, and was higher than −27 dB over the entire scanning frequency range.

# References

Alcheikh N, Xavier P, Duchamp JM, Schuster KF, Malhaire C, Remaki B, Boucher C, Mescot X (2014) Temperature dependence of the electromechanical characteristics of superconducting RF-MEMS switches. Microsyst Technol 21:1–7

Chiou JC, Chou LC, Lai YL, Huang SC (2012) A novel thermal switch and variable capacitance implement by CMOS MEMS process approaching in micro electrostatic converter. Solid State Electron 77:56–63

Deng PG, Lee YK, Lin R, Zhang TY (2012) Nonlinear electro-mechanobiological behavior of cell membrane during electroporation. Appl Phys Lett 10:053702

Deng PG, Lee YK, Zhang TY (2014) A nonlinear electromechanical coupling model for electropore expansion in cell electroporation. J Phys D Appl Phys 47:445401–445411

Gilbert KW, Mall S, Leedy KD, Crawford B (2008) A nanoindenter based method for studying MEMS contact switch microcontacts. In: Proceedings of the 54th IEEE holm conference on electrical contacts 2008, pp 137–144

Jaafar H, Beh KS, Yunus NAM, Hasan WZW, Shafie S, Sidek O (2014) A comprehensive study on RF MEMS switch. Microsyst Technol 20:2109–2121

Jan MT, Hamid NHB, Khir MHM, Ashraf K, Shoaib M (2014) Reliability and fatigue analysis in cantilever-based mems devices operating in harsh environments. J Qual Reliab Eng. doi:10.1155/2014/987847

Jang Y, Kang S, Kim HC, Chun K (2011) An RF MEMS switch with a differential gap between electrodes for high isolation and low voltage operation. J Micromech Microeng 21:75016–75024

Lii LR, Murphy KD (2010) Impact dynamics of MEMS switches. Nonlinear Dynam 60:327–339

Mafinejad Y, Zarghami M, Kouzani AZ (2013) Design and simulation of high isolation RF MEMS shunt capacitor switch for C–K band. Ieice Electron Expr 10:2347–2351

Mercado LL, Koo SM, Lee TYT, Liu L (2003) A mechanical approach to overcome RF MEMS switch stiction problem. In: IEEE electronic components and technology conf. 2003, pp 377–384

Mulloni V, Lorenzelli L, Margesin B, Barbato M, Meneghesso G (2016) Temperature as an accelerating factor for lifetime estimation of RF-MEMS switches. Microelectron Eng 160:63–67

Muniraj NJR, Sathesh K (2011) Design of MEMS switch for RF applications. Microsyst Technol 17:161–163

Newman HS, Ebel JL, Judy D, Maciel J (2008) Lifetime measurements on a high-reliability RF-MEMS contact switch. IEEE Microw Wireless Compon Lett 18:100–102

Oberhammer J, Stemme G (2006) Active opening force and passive contact force electrostatic switches for soft metal contact materials. J Microelectromech Syst 15:1235–1242

Pamidighantam S, Puers R, Baert K, Tilmans HAC (2002) Pull-in voltage analysis of electrostatically actuated beam structures with fixed-fixed and fixed-free end conditions. J Micromech Microeng 12:458–464

Pirmoradi E, Mirzajani H, Ghavifekr HB (2015) Design and simulation of a novel electro-thermally actuated lateral RF MEMS latching switch for low power applications. Microsyst Technol 21:465–475

Pisheh HS, Kim JM, Rebeiz GM (2009) A novel stress-gradient-robust metal-contact switch. IEEE MEMS 2009:27–30

Rebeiz GM (2003) RF MEMS: theory, design, and technology. Wiley, New York

Schimkat J (1999) Contact measurement providing basic design data for microrelay actuators. Sens Actuators A Phys 73(1–2):138–143

Shankar D, Mohd I, Ramjay P, Jain KK, Chatterjee R (2011) Effect of residual stress on RF MEMS switch. Microsyst Technol 17:1739–1745

Sim SM, Lee Y, Jang YH, Lee YS, Kim YK, Ignacio LG, Kim JM (2016) A 50–100 GHz ohmic contact SPDT RF MEMS silicon switch with dual axis movement. Microelectron Eng 162:69–74

Toler BF, Coutu RA, Mcbride JW (2013) A review of micro-contact physics for microelectromechanical systems metal contact switches. J Micromech Microeng. doi:10.1088/0960-1317/23/10/103001

Yuan XL, Huang QA, Liao XP (2008) Analysis of electromagnetic interference of a capacitive RF MEMS switch during switching. Microsyst Technol 14:349–360